PERGAMON

International Journal of Plasticity 19 (2003) 883–905

INTERNATIONAL JOURNAL OF Plasticity

www.elsevier.com/locate/ijplas

Modeling of cyclic mobility in saturated cohesionless soils

Ahmed Elgamal[a,*], Zhaohui Yang[a], Ender Parra[b], Ahmed Ragheb[c]

[a]*Department of Structural Engineering, University of California, San Diego, La Jolla, CA 92093, USA*
[b]*INTEVEP, SA, Venezuela*
[c]*Construction and Building Engineering Department, Arab Academy for Science and Technology, Egypt*

Received in final revised form 14 February 2002

Abstract

Cyclic mobility is exhibited by saturated medium to dense cohesionless soils during liquefaction, due to soil skeleton dilation at large shear strain excursions. This volume-shear coupling mechanism results in phases of significant regain in soil shear stiffness and strength, and limits the magnitude of cyclic shear deformations. Motivated by experimental observations, a plasticity model is developed for capturing the characteristics of cyclic mobility. This model extends an existing multi-surface plasticity formulation with newly developed flow and hardening rules. The new flow rule allows for reproducing cyclic shear strain accumulation, and the subsequent dilative phases observed in liquefied soil response. The new hardening rule enhances numerical robustness and efficiency. A model calibration procedure is outlined, based on monotonic and cyclic laboratory sample test data.

Keywords: Liquefaction; Cyclic mobility; Multi-surface plasticity; Soil mechanics; Constitutive modeling; Earthquake; Dilation; Granular material; Constitutive behaviour; Anisotropy; Kinematic hardening

1. Introduction

Liquefaction of soils (excess pore pressure ratio $r_u = u_e / \sigma'_v$ approaching and reaching 1.0, where u_e = excess pore pressure and σ'_v is effective vertical stress) and associated deformations remain among the main causes of damage during earth-

* Corresponding author. Tel.: +1-858-822-1075; fax: +1-858-822-2260.
E-mail address: elgamal@ucsd.edu (A. Elgamal).

0749-6419/03/$ - see front matter
PII: S0749-6419(02)00010-4

quakes (Seed et al., 1990; Bardet et al., 1995; Sitar, 1995; Japanese Geotechnical Society, 1996; Ansal et al., 1999; see also http://peer.berkeley.edu/turkey/adapazari). Indeed, dramatic unbounded deformations (flow failure) due to liquefaction in dams and other structures (Seed et al., 1975, 1989; Davis and Bardet, 1996) have highlighted the significance of this problem in earthquake engineering research. However, liquefaction more frequently results in limited, albeit possibly high levels of deformation (Casagrande, 1975; Youd et al., 1999). For instance (Hatanaka et al., 1997), the response of high quality (relatively undisturbed) samples of Masado soil is seen (Fig. 1) to demonstrate this mechanism (this soil developed major liquefaction-induced deformations during the 1995 Kobe, Japan earthquake). In such situations, the deformation process is mainly a consequence of limited-strain cyclic deformations (Seed, 1979), commonly known as cyclic mobility (Castro and Poulos, 1977) or cyclic liquefaction (Casagrande, 1975).

A large number of computational models have been, and continue to be developed for simulation of nonlinear soil response, and the dilatancy (shear-volume coupling) effects (e.g., DiMaggio and Sandler, 1971; Finn et al., 1977; Nemat-Nasser and Shokooh, 1979; Prevost, 1985, 1989; Dafalias, 1986; Pastor and Zienkiewicz, 1986; Anandarajah, 1993; Bardet et al., 1993; Muraleetharan et al., 1994; Byrne and McIntyre, 1994; Oka et al., 1995, 2002; Manzari and Dafalias, 1997, Cubrinovski and Ishihara, 1998; Borja et al., 1999a,b; Jeremic et al., 1999; Peric and Ayari, 2000, 2002; Li and Dafalias, 2000; Vaunat et al., 2000; Arduino et al., 2001; Nemat-Nasser and Zhang, 2002; Voyiadjis and Kim, 2002). Currently, reliable computational modeling of cyclic-mobility shear deformations still remains a major challenge. The research presented in this paper aims to develop a computational model for analysis of cyclic mobility scenarios. In this regard, emphasis is placed on more accurate reproduction of accumulated shear deformations in clean medium-dense cohesionless soils. Such accuracy is of utmost practical significance in structural/foundation stability and damage assessments. The developed constitutive model can be used within general fully coupled (solid–fluid) finite element formulations.

2. Cyclic mobility mechanism

In general, during a shear loading process near liquefaction (low confinement levels), a saturated undrained cohesionless soil exhibits the following pattern of behavior (Lambe and Whitman, 1969; Ishihara, 1985):

1. At low shear strains, the soil skeleton experiences a tendency for contraction (phase 0–1 in Fig. 2), leading to development of excess pore-pressure and reduction in effective confinement.
2. As the shear stress approaches the failure envelope, or more precisely the so-called Phase Transformation (PT) envelope (Ishihara, 1985; Iai, 1991; Vaid and Thomas, 1995; Vaid and Sivathayalan, 1999), significant shear strain may develop without appreciable change in shear stress (essentially, the perfectly plastic phase 1–2 in Fig. 2). Numerical versatility is achieved by defining

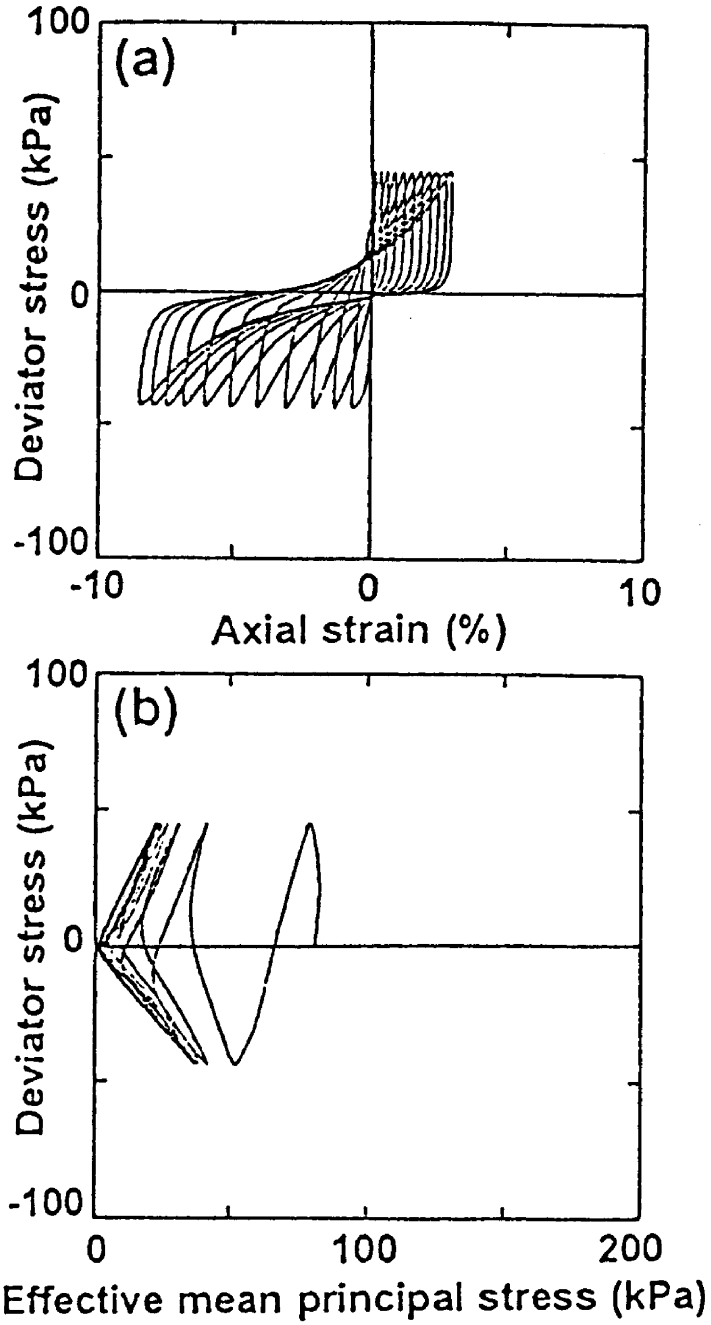

Fig. 1. Stress–strain relationship and stress path for undrained cyclic triaxial test on reclaimed gravely fill Masado soil (Hatanaka et al., 1997), which developed major liquefaction-induced deformations during the 1995 Kobe, Japan earthquake.

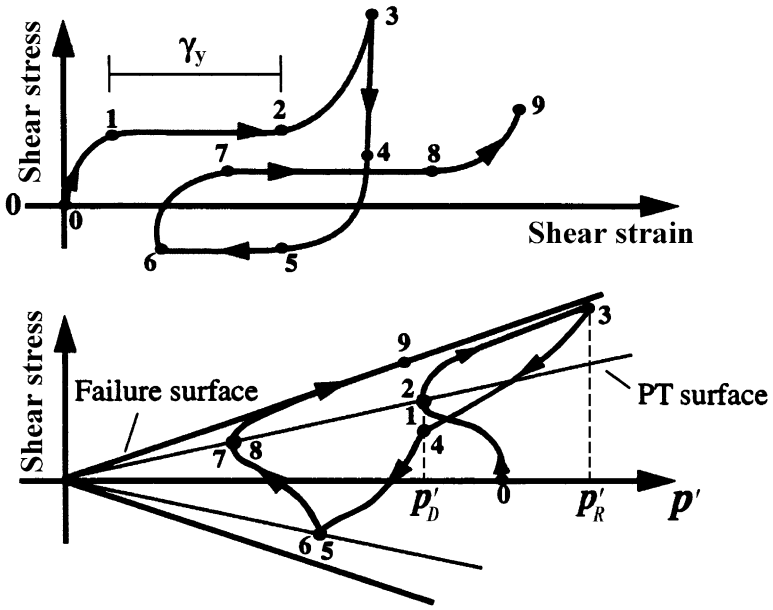

Fig. 2. Schematic of constitutive model response showing shear stress, effective confinement, and shear strain relationship.

this highly yielded segment of stress-strain response as a distinct phase (γ_y as shown in Fig. 2, where $\gamma = \sqrt{2/3\boldsymbol{e}:\boldsymbol{e}}$ refers to octahedral shear strain, and $\boldsymbol{e}$ = deviatoric strain tensor). This feature allows for direct control over the extent of shear strain accumulation.

3. Thereafter (above the PT envelope), a dilative tendency (phase 2–3 in Fig. 2) increases effective confinement (and consequently shear stiffness and strength), allowing the soil to resist increased levels of shear stress (by moving along the failure envelope).

For the purpose of liquefaction-induced shear deformations, medium-dense clean granular soils are found to exhibit the above-described response. A survey of experimental research (triaxial and shear tests) compiled by Seed (1979) suggested that such clean sands, with a relative density D_r of about 45% or more, appeared to exhibit the mechanism of limited strain cyclic mobility during liquefaction. More recent laboratory experiments (e.g., Ishihara, 1985; Arulmoli et al., 1992; Boulanger and Seed, 1995; Sture, 1999), shake-table, and centrifuge tests (Dobry et al., 1995; Dobry and Abdoun, 1998; Balakrishnan and Kutter, 1999) continue to corroborate the findings of earlier studies (in clean sands and non-plastic silts). In such experimental observations, uniform cohesionless soils with a reported D_r of as low as 37%, may accumulate large liquefaction-induced cyclic shear strains, but do not exhibit flow-type failures (see Elgamal et al., 1998 for an extensive literature survey).

3. Constitutive model

Accurate accounting of the above-mentioned response characteristics is the main objective of the current study. Our plasticity model (Parra, 1996; Yang, 2000) is based on the original framework of Prevost (1985), in which a multi-surface approach is adopted for cyclic hysteretic response (Iwan, 1967; Mroz, 1967). In this model, the contractive, perfectly plastic, and dilative phases of Fig. 2 were incorporated by developing a new appropriate flow rule. The incorporated new flow rule significantly changes the characteristics of model response, in order to reproduce the salient cyclic mobility mechanisms (Figs. 1 and 2), and exercise more direct control over shear strain accumulation (in accordance with experimental observations). In addition, a new hardening rule was developed for more robust and efficient numerical performance.

In the following sections, after a brief description of the yield surface configuration, focus will be placed on the new developments. According to the sign convention commonly used in soil mechanics, volumetric stresses and strains are positive in compression.

3.1. Yield function

The yield function f (Fig. 3) is selected of the following form (Prevost, 1985):

$$f = \frac{3}{2}\left(\boldsymbol{s} - \left(p' + p'_0\right)\boldsymbol{\alpha}\right) : \left(\boldsymbol{s} - \left(p' + p'_0\right)\boldsymbol{\alpha}\right) - M^2\left(p' + p'_0\right)^2 = 0 \tag{1}$$

in the domain of $p' \geqslant 0$, where $\boldsymbol{s} = \boldsymbol{\sigma}' - p'\ \boldsymbol{\delta}$ is the deviatoric stress tensor ($\boldsymbol{\sigma}'$ = effective Cauchy stress tensor, $\boldsymbol{\delta}$ = second-order identity tensor), p' is mean effective stress, p'_0 is a small positive constant (2.0 kPa in this paper) such that the yield surface size remains finite at $p' = 0$ (for numerical convenience and to avoid

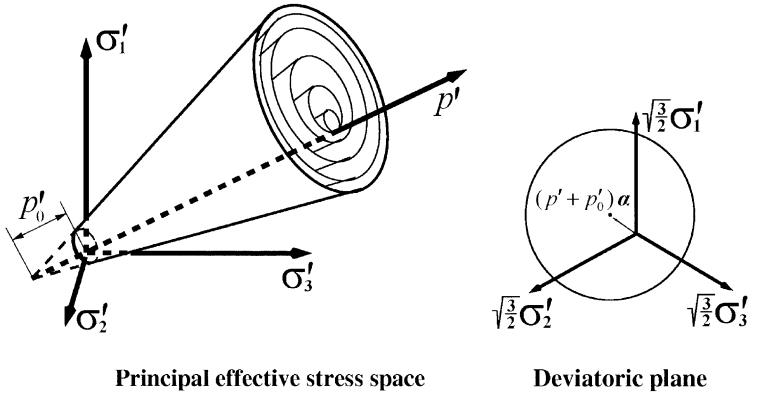

Fig. 3. Conical yield surface in principal stress space and deviatoric plane (after Prevost, 1985; Parra, 1996; Yang, 2000).

ambiguity in defining the yield surface normal at the yield surface apex, Fig. 3), $\boldsymbol{\alpha}$ is second-order kinematic deviatoric tensor defining the yield surface coordinates, M dictates the yield surface size (defined by friction angle for the outmost surface), and ":" denotes doubly contracted scalar product of two tensors. In the context of multi-surface plasticity, a number of similar yield surfaces with a common apex and different sizes form the hardening zone (Fig. 3). Each surface is associated with a constant plastic modulus. The outmost surface is designated as the failure surface. As usually postulated (Prevost, 1985), the low-strain (elastic) moduli and plastic yield surface moduli increase in proportion to the square root of effective confinement.

It is realized that the employed yield surface is open in the positive direction of hydrostatic axis (Fig. 3). One may introduce a cap yield function (e.g., DiMaggio and Sandler, 1971; Lacy, 1986; Wang et al., 1990) to close the open end. As indicated by Manzari and Dafalias (1997), under normal confining pressures of interest in geotechnical engineering, a stress path along the positive branch of the hydrostatic axis induces relatively small strains. Thus, for shear-dominated load paths (such as earthquake excitation), many researchers have opted to maintain a level of simplicity, and do without a cap function (e.g., Prevost, 1985; Manzari and Dafalias, 1997; Li and Dafalias, 2000). In general, cyclic loading data for calibration of cap-type yield functions is scarce, and significant research is needed within the multi-surface context (Lacy, 1986).

3.2. Flow rule

Within the theory of plasticity framework, the phenomenological interaction between shear and volume change (contraction or dilation) is typically handled by specifying an appropriate non-associative flow rule (e.g., Prevost, 1985; Dafalias, 1986; Bousshine et al., 2001; Nemat-Nasser and Zhang, 2002; Radi et al., 2002). In the current model, the deviatoric component of the flow rule is associative, and nonassociativity is restricted to the volumetric component only (similar to earlier formulations).

Denoting $\boldsymbol{P}$ as the direction of plastic flow, its volumetric component P'' defines the desired level of dilation or contraction in accordance with experimental observation. Consequently, P'' is defined by (Prevost, 1985; Parra, 1996):

$$3P'' = \frac{1-(\eta/\bar{\eta})^2}{1+(\eta/\bar{\eta})^2}\Psi \tag{2}$$

where $\eta = \sqrt{(3/2)\boldsymbol{s}:\boldsymbol{s}}/\left(p'+p'_0\right)$ is effective stress ratio, $\bar{\eta}$ a material parameter defining the stress ratio of the PT surface (see Section 2), and Ψ a newly introduced scalar-valued function (Parra, 1996; Yang, 2000) for controlling the magnitudes of dilation and contraction, as described below (a scalar material parameter was used in Popescu and Prevost (1993) in place of the function Ψ). Note that if $(1-(\eta/\bar{\eta})^2)$ is positive, the stress state lies within the PT surface, and if negative, the stress state lies above the PT surface. In addition, loading corresponds to an increasing η, and unloading corresponds to a decreasing η.

3.2.1. Within phase transformation surface (phase 0-1, Fig. 2)

Within the PT surface, contraction always takes place irrespective of loading/unloading condition. The contraction scaling function in Eq. (2) is chosen to be (Parra, 1996):

$$\Psi = c_1 \exp(c_2 p'/P_a) \tag{3}$$

where c_1 and c_2 are two material constants dictating the rate of contraction (or equivalently, the rate of excess pore-pressure buildup under undrained condition), and P_a is atmospheric pressure (101 kPa, used as a normalization constant). The parameter c_1 depends on the particular soil type and relative density (larger c_1 values correspond to stronger contraction), and c_2 allows for a form of confinement dependence if deemed necessary.

3.2.2. On phase transformation surface (phase 1–2, Fig. 2)

The point at which the stress path intersects the PT surface is denoted as point D (Fig. 2) and the effective confinement p'_D is stored as a temporary material memory parameter (Parra, 1996). At low confinement levels near liquefaction, a constant-volume perfectly plastic phase is activated and the stress state remains at D, until a user-defined octahedral shear strain increment γ_y is accumulated (Fig. 2). As shown in Fig. 4, the introduction of γ_y offers significant versatility in controlling the magnitude of near- and post-liquefaction yielding response (this yield phase is only significant at low confinement of 10 kPa or less based on existing data). For the important situation of accumulation of shear strains in a preferred (down-slope) direction (e.g., mildly inclined strata or infinite slope, below and around embankments or foundations, and other lateral spreading situations), γ_y conveniently allows down-slope deformations to accumulate in a controlled fashion during each additional loading cycle (phase 7–8 in Fig. 2). This feature is of utmost practical importance.

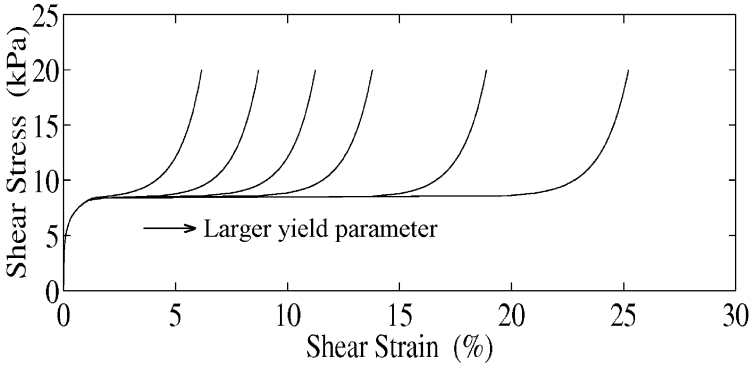

Fig. 4. Yield phase performance as a function of the yield parameter γ_y.

Specifically, the parameter γ_y is defined by:

$$\gamma_y = y_1 + y_2 \ \gamma_T \tag{4}$$

where γ_T is total octahedral plastic strain accumulated during liquefaction ($\gamma_T = \int_0^t \gamma^p \mathrm{d}t$ where t is time), and y_1 and y_2 are user-defined material constants (Fig. 4). A larger y_1 is typically needed for a looser soil. In addition, y_2 can be used to extend the yielding phase γ_y from one cycle to the next (a cumulative damage-type effect, e.g., Chiarelli and Shao, 2002).

3.2.3. Above phase transformation surface, loading (phase 2-3, Fig. 2)

Upon the accumulation of γ_y, a sharp dilation tendency is activated (compared to earlier formulations, Prevost, 1985; Popescu and Prevost, 1993). The dilation scaling function in Eq. (2) is defined by (Parra, 1996):

$$\Psi = d_1 \exp(d_2 \ \gamma_d) \tag{5}$$

where d_1 and d_2 are material constants, and γ_d is cumulative octahedral plastic strain during the current dilative phase. Larger d_1 and d_2 values result in increasingly stronger dilation, eventually limited by the conical yield surface gradient (associated flow). Eq. (5) allows the dilation tendency to increase progressively, and significantly reduces further straining (Fig. 5). The increase in shear stress and effective confinement due to dilation may be limited by (Casagrande, 1975): (a) reaching the critical void-ratio (or constant-volume) state at large shear strain (Li and Dafalias, 2000), or (b) fluid cavitation (i.e., pore water pressure reduced to -1 atmospheric pressure).

3.2.4. Above phase transformation surface, unloading (phase 3-4, Fig. 2)

A different definition of P'' is needed (Parra, 1996) to allow for a swift return to the confinement level p'_D upon unloading (phase 3-4, Fig. 2). For that purpose, the following relationship resulted in satisfactory performance:

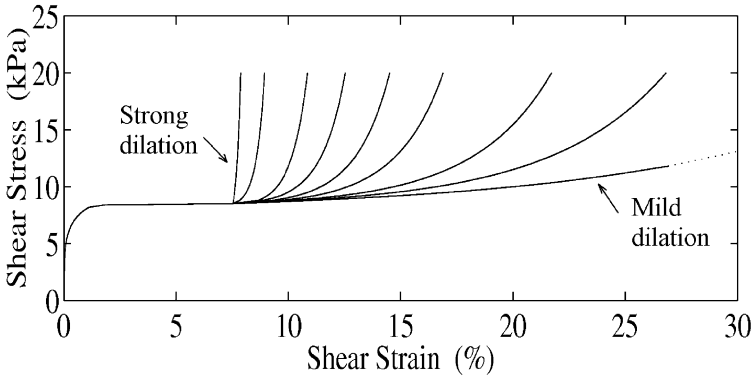

Fig. 5. Dilation function performance for a given γ_y and different user-defined rates of dilation.

$$\frac{\sqrt{3/2\boldsymbol{P}' : \boldsymbol{P}'}}{P''} = \frac{p'_D}{p'_R}\eta_f \tag{6}$$

in which $\boldsymbol{P}'$ is deviatoric component of the tensor $\mathbf{P}$, η_f is stress ratio along the failure surface, and p'_R is effective confinement at the load reversal point R (Fig. 2). This rule relates the rate of contraction to the extent of accumulated confinement (distance between p'_R and p'_D, Fig. 2). Representative performance of unloading behavior is shown in Fig. 6. Once confinement decreases to the level of point D, p'_D is no longer a memory parameter, and the contraction logic within the PT surface takes over. Dependence of contraction on earlier dilation conforms with experimental observations (Nemat-Nasser and Tobita, 1982), as also represented in the models of Dafalias and Manzari (1999) and Nemat-Nasser and Zhang (2002).

It is noted that the above newly developed non-associative rules obey the requirement of positive plastic dissipation (Lubliner, 1990; Brannon, 2002). In addition, the Kuhn–Tucker conditions are satisfied (Lubliner, 1990).

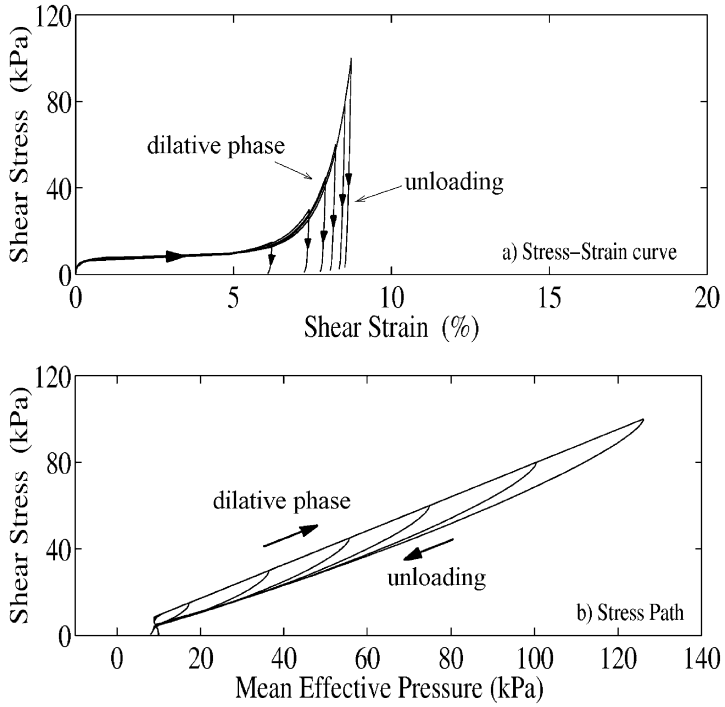

Fig. 6. Unloading function performance at different levels of dilation (dilation-induced shear strength and effective confinement return to the pre-dilation levels).

3.3. Hardening rule

A purely deviatoric kinematic hardening rule is employed (Prevost, 1985), to conveniently generate hysteretic cyclic response. In the context of multi-surface plasticity, translation of the yield surface is generally governed by the consideration that no overlapping is allowed between yield surfaces (Mroz, 1967). Thus, contact between consecutive similar surfaces f_m and f_{m+1} (Fig. 7) must occur only at conjugate points with the same direction of outward normal. In this regard, Mroz (1967) proposed using the current (deviatoric) stress state **s** on the active surface f_m (Fig. 7) and its conjugate point R on the next outer surface f_{m+1}, to define the translation direction $\boldsymbol{\mu}$ as follows (Fig. 7):

$$\boldsymbol{\mu} = \frac{M_{m+1}}{M_m}\left[\boldsymbol{s} - \left(p' + p'_0\right)\boldsymbol{\alpha}_m\right] - \left[\boldsymbol{s} - \left(p' + p'_0\right)\boldsymbol{\alpha}_{m+1}\right] \tag{7}$$

where $\left(p' + p'_0\right)\boldsymbol{\alpha}_m$ and $\left(p' + p'_0\right)\boldsymbol{\alpha}_{m+1}$ are the centers of f_m and f_{m+1} respectively in the deviatoric plane. The trajectory of translation is shown as the shadowed zone in Fig. 7. With the direction of translation defined, the amount of translation $\mathrm{d}\mu$ may then be obtained by satisfying the consistency condition $\dot{f} = 0$ (Mroz, 1967). After updating the active surface f_m, all inner surfaces are translated to be tangential at the updated stress state $(\boldsymbol{s} + \mathrm{d}\boldsymbol{s})$ on f_m. The translation rule of Eq. (7) was subsequently adopted by Dafalias and Popov (1975) in two-surface models, and by Prevost (1978a,b, 1985) in multi-surface model formulations.

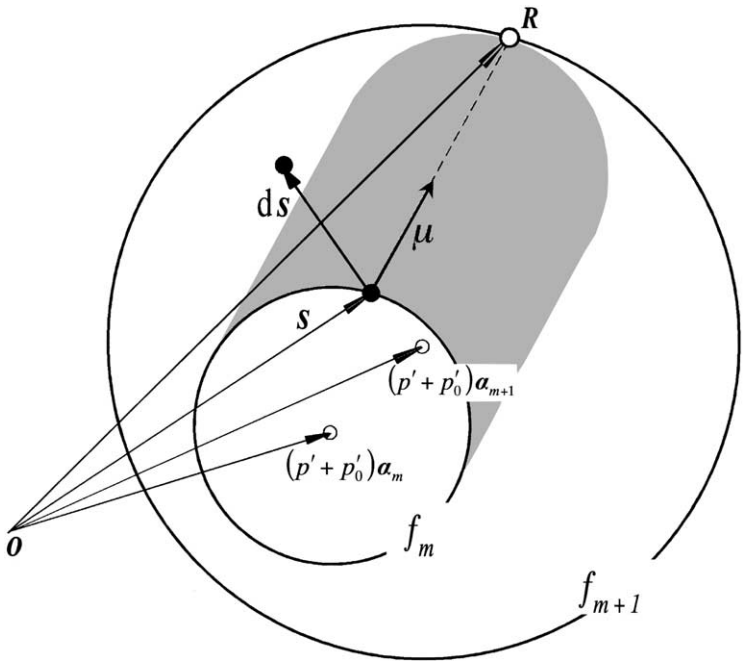

Fig. 7. Mroz (1967) deviatoric hardening rule.

In our numerical implementation experience, Mroz's rule [Eq. (7)] was found to demand a high level of computational effort under certain loading conditions. This was particularly evident at low confinement levels where yield surfaces are of increasingly small size in the deviatoric plane. In such cases, even with relatively small stress increments, the updated stress state ($\mathbf{s}+\mathrm{d}\mathbf{s}$) may still lie outside the trajectory of inner surface translation (Fig. 7), and the consistency condition cannot be satisfied. Use of smaller load increments to remedy this problem was found to be prohibitively expensive (e.g., in Boundary Value Problem Finite Element computations), and sometimes practically impossible.

In view of the above, a new translation rule $\boldsymbol{\mu}$ (Fig. 8) was defined (Parra, 1996):

$$\boldsymbol{\mu} = \left[\boldsymbol{s}_T - \left(p' + p'_0\right)\boldsymbol{\alpha}_m\right] - \frac{M_m}{M_{m+1}}\left[\boldsymbol{s}_T - \left(p' + p'_0\right)\boldsymbol{\alpha}_{m+1}\right] \tag{8}$$

where s_T is the deviatoric stress tensor defining the position of point T (Fig. 8) as the intersection of f_{m+1} with the vector connecting the inner surface center $\left(p' + p'_0\right)\boldsymbol{\alpha}_m$ and the updated stress state ($\boldsymbol{s}+\mathrm{d}\boldsymbol{s}$). This rule [Eq. (8)] is also based on the Mroz (1967) conjugate-points concept, and allows no overlapping of yield surfaces. Use of point T to define conjugate points eliminated the numerical challenges mentioned above, as the updated stress state is now always within the inner surface translation trajectory.

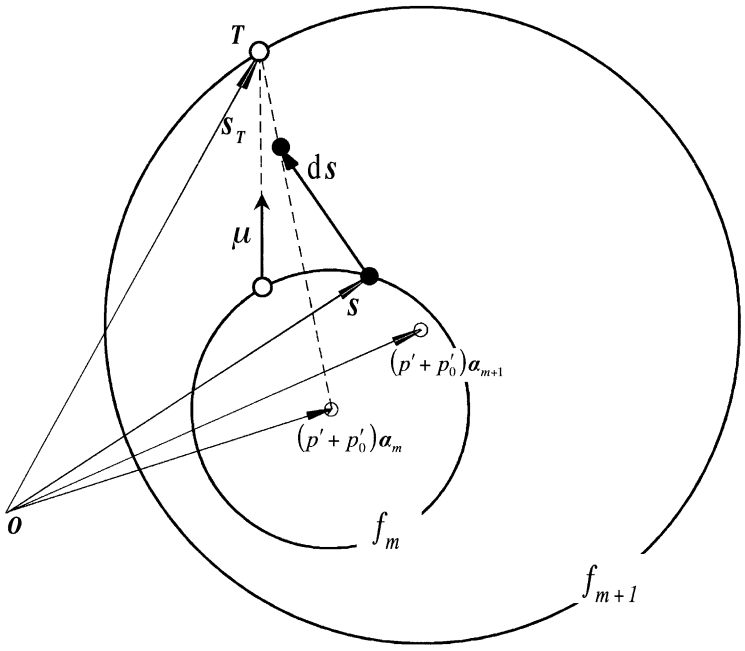

Fig. 8. New deviatoric hardening rule (after Parra, 1996).

Table 1
Major model parameters derived from calibration phase

Model parameter	Nevada No. 120 Sand at $D_r = 40\%$
Reference shear modulus (at $p = 80$ kPa)	3.3×10^4 kPa
Reference bulk modulus (at $p = 80$ kPa)	2.2×10^4 kPa
Friction angle	31.4°
Phase transformation angle	26.5°
Contraction parameter c_1	0.18
Contraction parameter c_2	1.0
Dilation parameter d_1	0.5
Dilation parameter d_2	100.0
Perfectly plastic strain parameter y_1	1.0%
Perfectly plastic strain parameter y_2	0.0

The concept of using the updated stress state to define a surface translation trajectory was employed earlier by Dafalias and Popov (1977), for an inner surface of vanishing size (vanishing elastic region in a bounding surface formulation). Finally, it is worth mentioning that the new translation rule also applies in stress subspaces where one or more stress components may be absent (proof follows that of Mroz, 1967).

3.3.1. Remarks

1. An explicit elastic predictor-return mapping approach is used for numerical integration of the constitutive equations (in which the deviatoric component obeys radial return), with an automatic strain sub-incrementation algorithm to improve accuracy (Parra, 1996).
2. The Lode angle effect (Hill, 1950; Lade, 1977) is not incorporated in the current model since the yield function [Eq. (1)] does not include the third

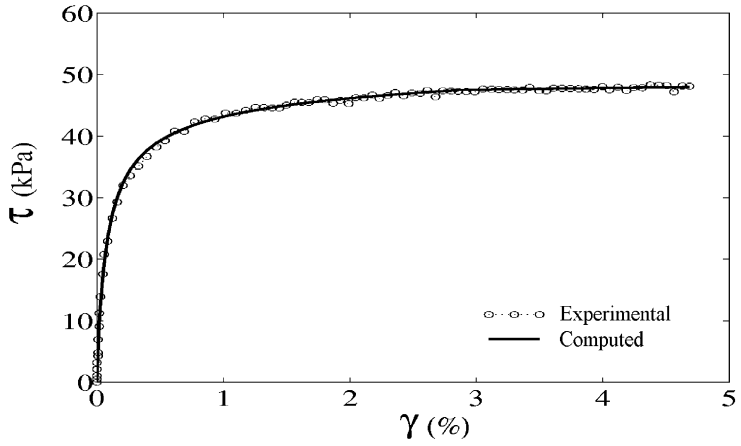

Fig. 9. Computed and laboratory (Arulmoli et al., 1992) stress–strain curves for an isotropically consolidated, drained monotonic triaxial loading test ($D_r = 40\%$, VELACS Test No. 40–100).

stress invariant. Load paths that depend significantly on this effect (e.g., circular loading, Peric and Ayari, 2000, 2002) will not be reproduced satisfactorily. Effort is currently directed towards inclusion of the third stress invariant in the yield function.

4. Model calibration and performance

4.1. Model calibration

The constitutive model was calibrated (pilot effort by Parra, 1996) by monotonic and cyclic laboratory sample test data in which Nevada No. 120 fine sand (D_r of

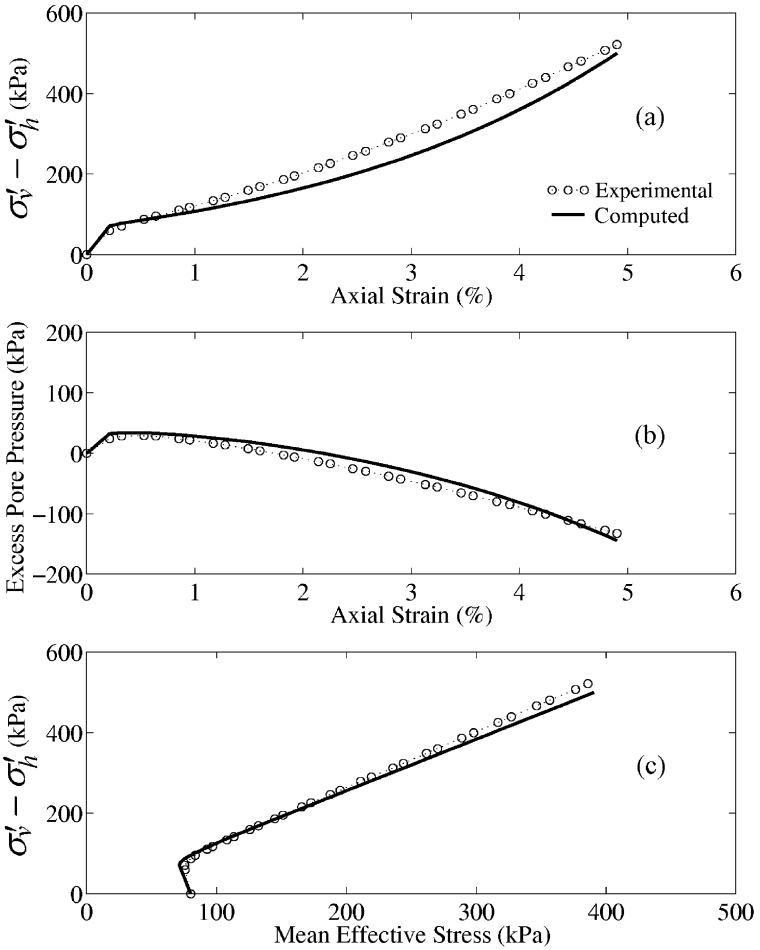

Fig. 10. Computed and laboratory (Arulmoli et al., 1992) results of an isotropically consolidated, undrained monotonic triaxial loading test ($D_r = 40\%$, VELACS Test No. 40–04).

about 40%) was employed (Arulmoli et al., 1992). In addition, a series of one-dimensional lateral spreading centrifuge experimental results (Dobry et al., 1995) is being employed for calibration. The goal was to obtain an overall reasonable match of all consistent experimental characteristics. Due to space limitation, only the laboratory-tests calibration results are presented below. Table 1 illustrates the model parameters as calibrated by these experimental data sets.

Fig. 9 shows the experimental and computed results of a monotonic drained triaxial laboratory test (Arulmoli et al., 1992) conducted at a mean effective confining pressure of 80 kPa (held constant throughout). In Fig. 9, τ and γ are octahedral shear quantities ($\tau = \sqrt{1/3\boldsymbol{s} : \boldsymbol{s}}$). Data from this type of experiment mainly serves as a basis for defining the low-strain (linear) soil shear stiffness, as well as the maximum shear strength (or friction angle) evaluated at the corresponding effective confining pressure.

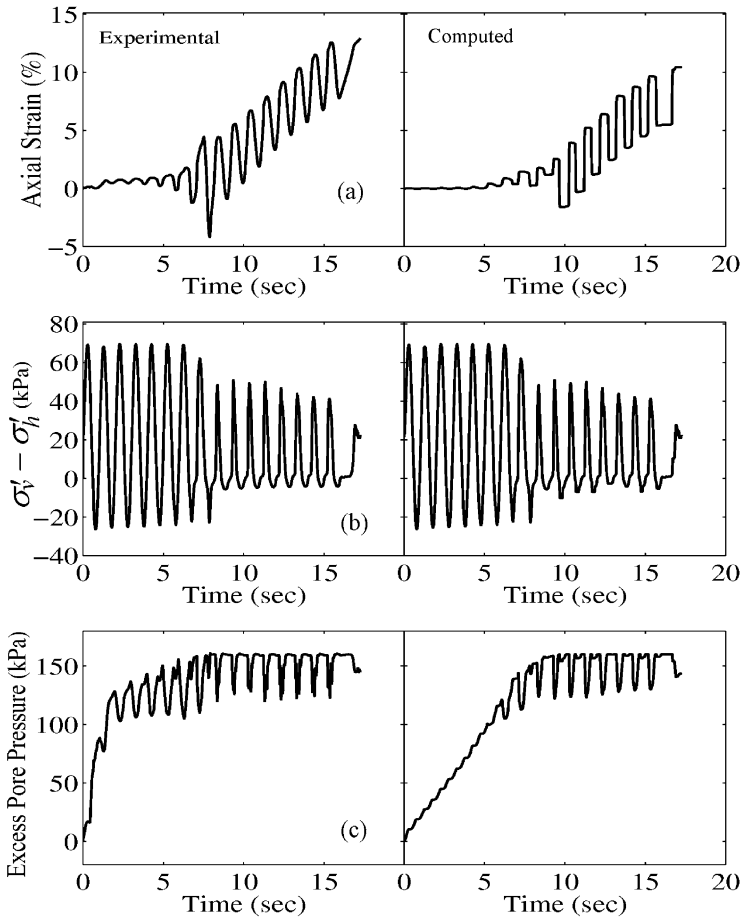

Fig. 11. Computed and laboratory (Arulmoli et al., 1992) results of an anisotropically consolidated, undrained cyclic triaxial loading test ($D_r = 40\%$, VELACS Test No. 40–58).

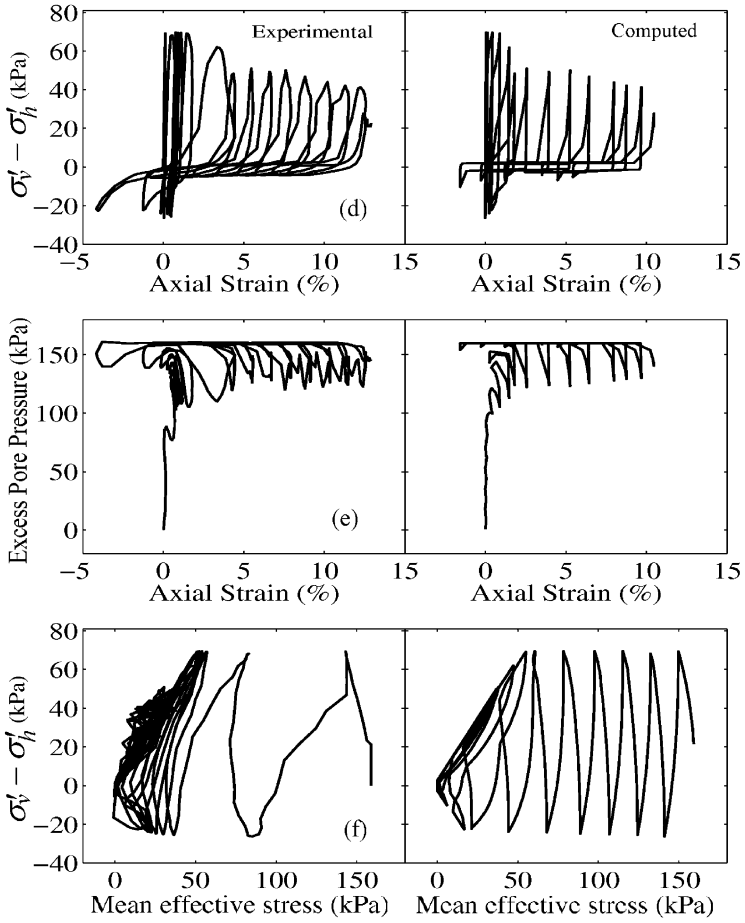

Fig. 11. (continued)

The experimental and computed results of a monotonic undrained triaxial test (Arulmoli et al., 1992) at an initial effective mean confinement of 80 kPa are shown in Fig. 10. Results of this type of experiment serve to define the model parameters c_1, c_2 [Eq. (3)], and d_1 and d_2 [Eq. (5)], that control contraction and dilation response, respectively.

Fig. 11 shows the experimental and computed results of an anisotropically consolidated, stress-controlled undrained cyclic triaxial test (initial vertical and horizontal normal stresses of $\sigma_v = 173$ kPa and $\sigma_h = 152$ kPa, Arulmoli et al., 1992). During cyclic loading, the sample gradually lost its effective confinement (Fig. 11f). Accordingly, excess pore pressure increased and eventually reached liquefaction (Fig. 11c). Due to the presence of the static stress bias ($\sigma_v(- \sigma_h)$, axial strain is seen to accumulate after liquefaction on a cycle-by-cycle basis (Fig. 11a), followed by a strong dilation tendency and associated regain in shear stiffness (Fig. 11d). The dilation phases resulted in instants of pore pressure drop (Fig. 11c).

It is noted that modeling the cyclic response pattern of Fig. 11d is among the primary goals of this constitutive modeling effort. In this calibration phase, load cycles were matched individually (Fig. 12). Results of this type of liquefaction experiment serve to define the model parameters y_1 and y_2 [Eq. (4)] that control the accumulation of liquefaction-induced cyclic yield strain (and also verify c_1, c_2, and d_1, d_2).

4.2. Model performance

Representative simulation results using the developed model are shown in Figs. 13 and 14. Model response in a strain-controlled undrained cyclic shear loading simulation shows that (Fig. 13): (i) the cyclic shearing process leads to a gradual buildup of pore pressure (Fig. 13c) with a corresponding decrease in effective confinement (Fig. 13f), and (ii) as excess pore pressure increases, soil gradually loses all shear stiffness and strength (Fig. 13e), and is unable to resist any appreciable shear loading (Fig. 13b,e).

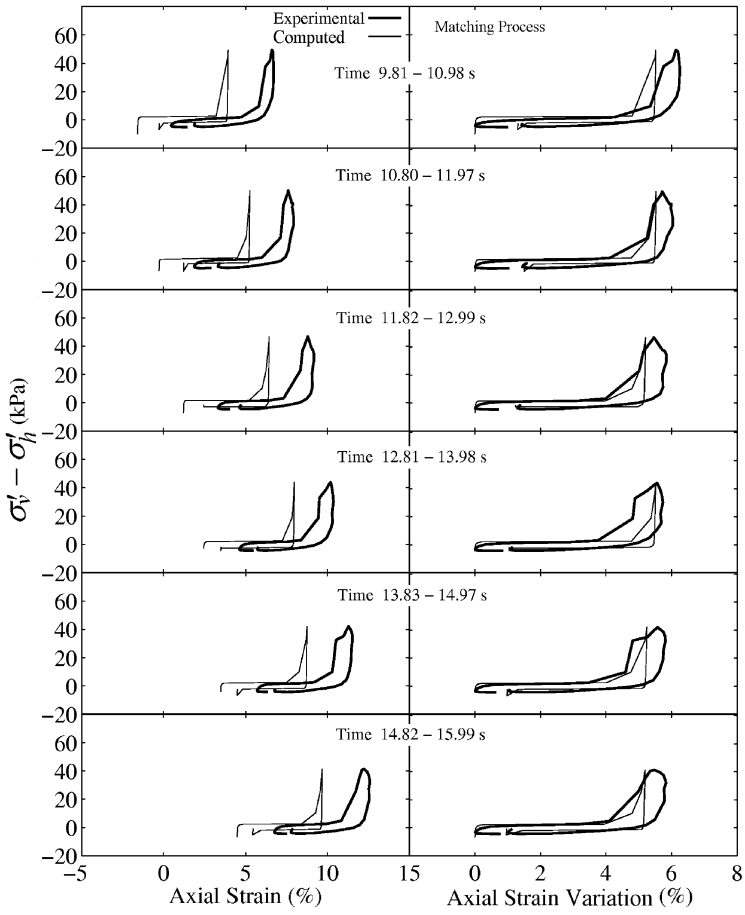

Fig. 12. Cycle-by-cycle matching between computed and measured post-liquefaction shear strain response of VELACS Test No. 40–58 ($D_r = 40\%$).

Fig. 14 depicts an undrained model response under symmetric stress-controlled cyclic shear loading. Again, pore pressure increases (Fig. 14c), and the reduction in overall shear stiffness and strength is clearly seen (Fig. 14e). As the soil liquefies, the amplitude of cyclic plastic deformation increases steadily in each loading cycle [Fig. 14a, dictated by the parameter y_2 in Eq. (4)], followed thereafter by a strong dilative response (Fig. 14e, f).

Finally, Fig. 15 depicts undrained model response under stress-controlled cyclic shear loading with a static shear stress bias, representative of an inclined soil slope (similar to Fig. 11). In this case, the computational model reproduces cycle-by-cycle accumulation of permanent deformation towards the down-slope direction.

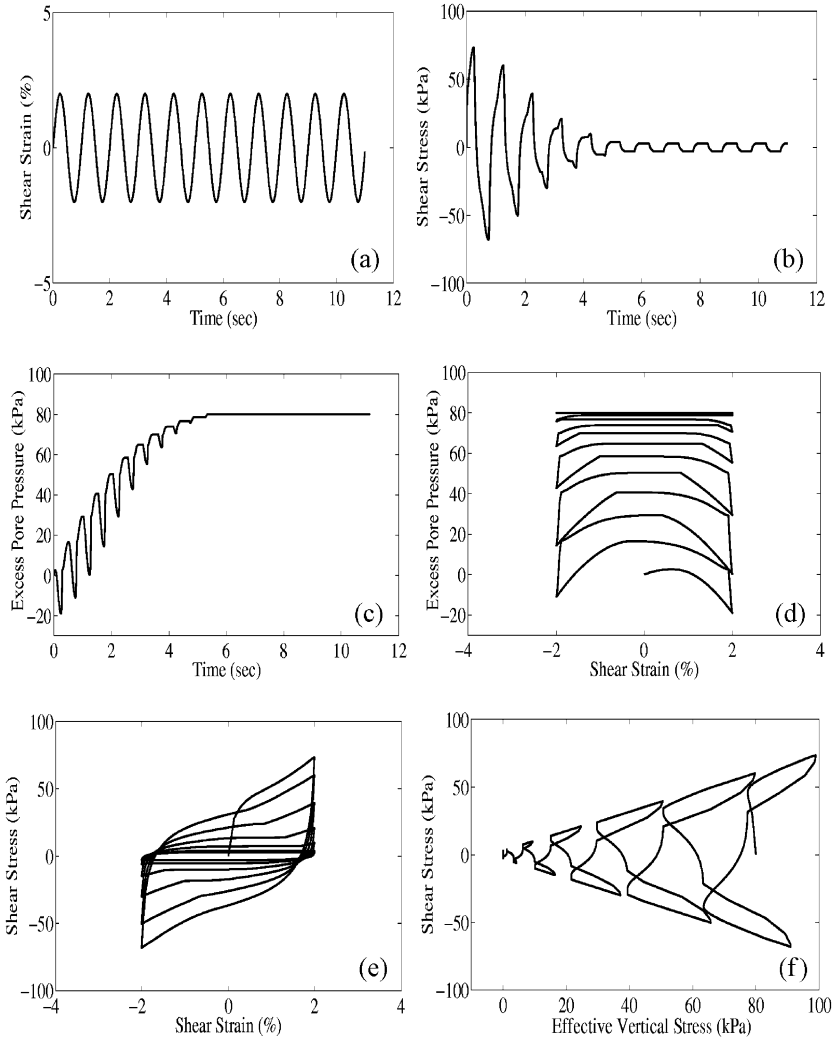

Fig. 13. Model simulation of strain-controlled, undrained cyclic shear loading (Parra, 1996).

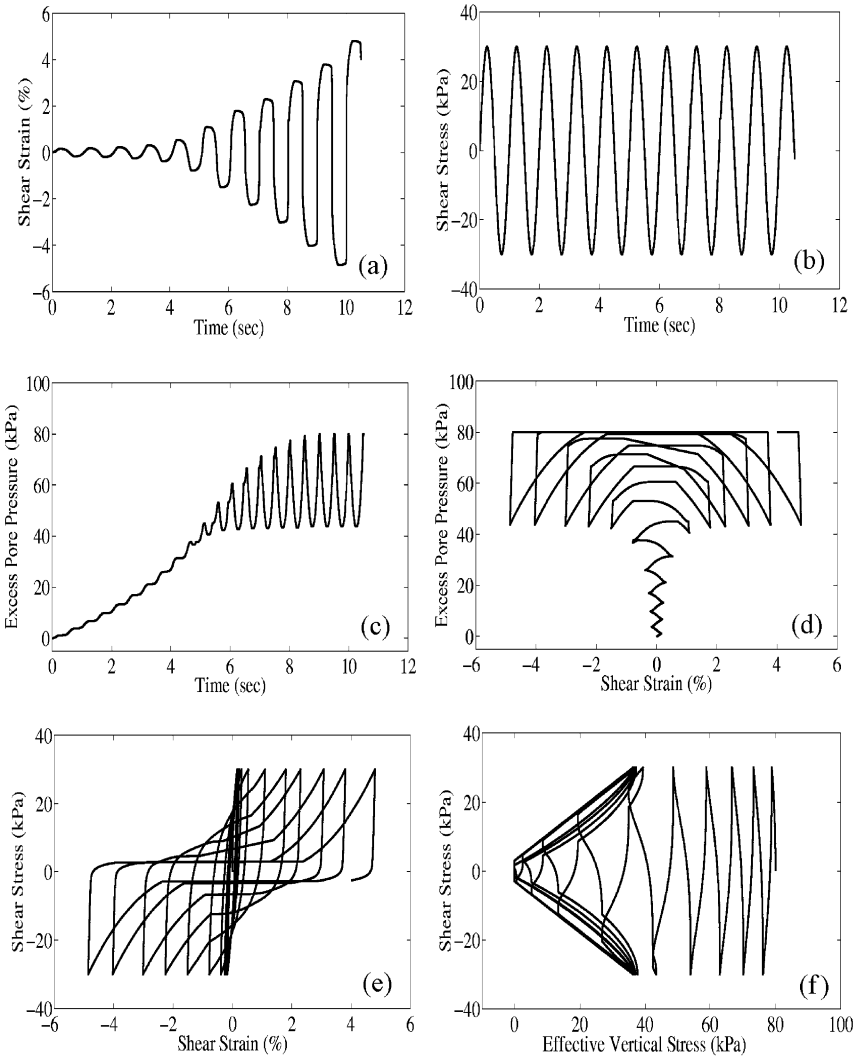

Fig. 14. Model simulation of stress-controlled, undrained cyclic shear loading (Parra, 1996).

5. Summary and conclusions

A constitutive model was developed for simulating the characteristics of cyclic mobility observed in saturated, medium to dense cohesionless soil response. Within a multi-surface plasticity framework, the new model incorporates shear-induced contractive, perfectly plastic, and dilative response phases implemented through an appropriate non-associative flow rule. The newly developed flow rule was motivated by experimental observations, and was defined to capture the involved phenomena. Emphasis was placed on accurately reproducing the development and accumulation

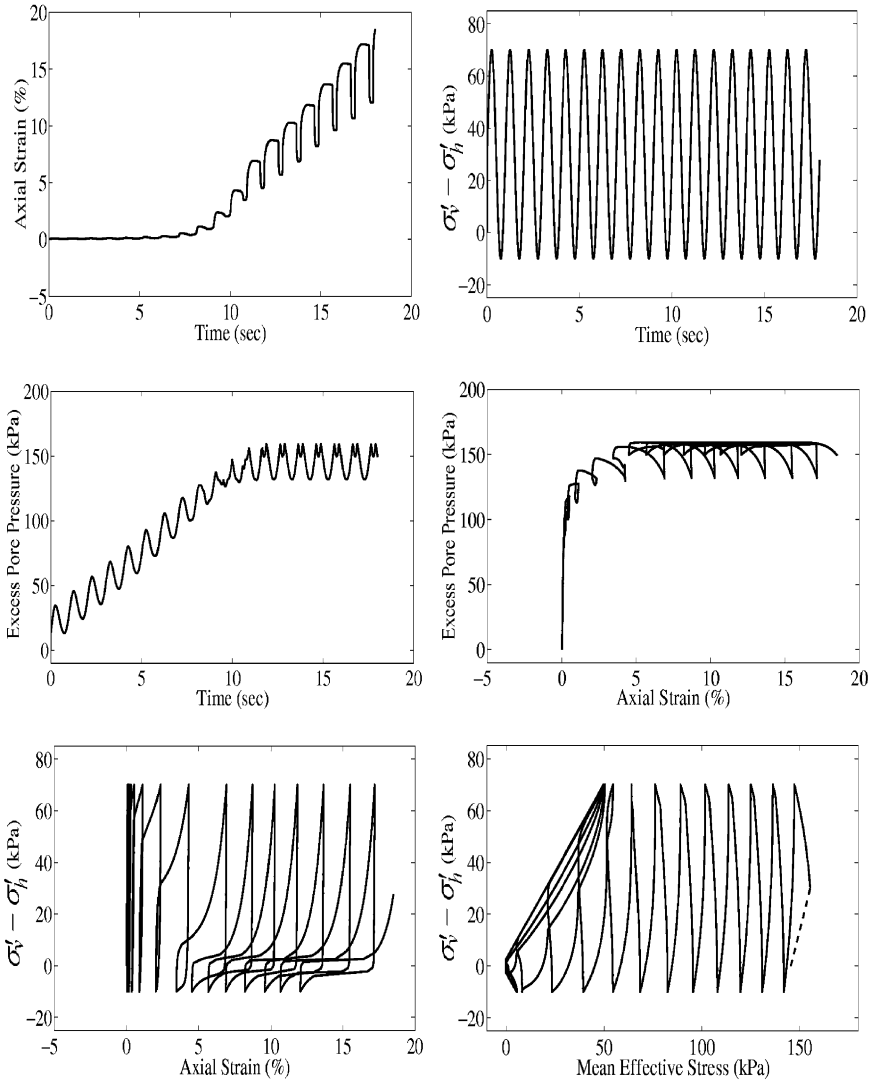

Fig. 15. Model simulation of stress-controlled, undrained cyclic shear loading with a static shear stress bias (Parra, 1996).

of shear deformations. A new hardening rule was also introduced to enhance numerical robustness and to increase efficiency. A model calibration procedure was outlined, based on monotonic and cyclic laboratory sample test data. Selected representative simulation results were presented to illustrate the salient model response characteristics. Further research work is needed primarily for more accurate modeling of plastic volumetric strains, and for including the Lode angle effect. Other refinements may be introduced, as new data sets become available.

Acknowledgements

The research reported herein was supported by the Pacific Earthquake Engineering Research (PEER) Center, through the Earthquake Engineering Research Centers Program of the National Science Foundation under Award Number EEC-9701568, by INTEVEP, SA, Venezuela, and by the National Science Foundation (grant No. CMS0084616). This support is gratefully acknowledged. The authors are indebted to Professor Sia Nemat-Nasser at U.C. San Diego for valuable discussions and advice.

References

Anandarajah, A., 1993. VELACS project: elasto-plastic finite element predictions of the liquefaction behavior of centrifuge models No. 1, 3 and 4a. In: Arulanandan, K., Scott, R.F. (Eds.), Proceedings of the International Conference on the Verification of Numerical Procedures for the Analysis of Soil Liquefaction Problems, Vol. 1. Balkema, Netherlands, pp. 45–66.

Ansal, A., Bardet, J.P., Barka, A., Baturay, M.B., Berilgen, M., Bray, J., Cetin, O., Cluff, L., Durgunoglu, T., Erten, D., Erdik, M., Idriss, I.M., Karadayilar, T., Kaya, A., Lettis, W., Olgun, G., Paige, W., Rathje, E., Roblee, C., Stewart, J., Ural, D., 1999. Initial Geotechnical Observations of the November 12, 1999, Düzce Earthquake. A Report of the Turkey-US Geotechnical Earthquake Engineering Reconnaissance Team, Nov. 26.

Arulmoli, K., Muraleetharan, K.K., Hossain, M.M., Fruth, L.S., 1992. VELACS: Verification of Liquefaction Analyses by Centrifuge Studies, Laboratory Testing Program, Soil Data Report. Project No. 90–0562. The Earth Technology Corporation, Irvine, CA.

Arduino, P., Kramer, S., Baska, D., 2001. UW-sand: a simple constitutive model for liquefiable soils. In: Book of Abstracts, 2001 Mechanics and Materials Summer Conference, 27–29 June, San Diego, CA, p. 108.

Balakrishnan, A., Kutter, B.L., 1999. Settlement, sliding and liquefaction remediation of layered soil. J. Geotechnical and Geoenvironmental Engineering, ASCE 125 (11), 968–978.

Bardet, J.P., Huang, Q., Chi, S.W., 1993. Numerical prediction for model no. 1. In: Arulanandan, K., Scott, R.F. (Eds.), Proceedings of the International Conference on the Verification of Numerical Procedures for the Analysis of Soil Liquefaction Problems, Vol. 1. Balkema, Netherlands, pp. 67–86.

Bardet, J.P., Oka, F., Sugito, M., Yashima, A., 1995. The Great Hanshin Earthquake disaster. Preliminary Investigation Report. Dept. of Civil Engineering. University of Southern California, Los Angeles, CA.

Borja, R.I., Chao, H.Y., Montans, F., Lin, C.H., 1999a. Nonlinear ground response at Lotung LSST site. J. Geotechnical and Geoenvironmental Engineering, ASCE 125 (3), 187–197.

Borja, R.I., Chao, H.Y., Montans, F., Lin, C.H., 1999b. SSI effects on ground motion at Lotung LSST site. J. Geotechnical and Geoenvironmental Engineering, ASCE 125 (9), 760–770.

Boulanger, R.W., Seed, R.B., 1995. Liquefaction of sand under bidirectional monotonic and cyclic loading. J. Geotechnical Engineering, ASCE 121 (12), 870–878.

Bousshine, L., Chaaba, A., Saxcé, G.De, 2001. Softening in stress-strain curve for Drucker-Prager non-associated plasticity. Intl. J. Plasticity 17 (1), 21–46.

Brannon, R.M. Prevention of negative plastic work in porous plasticity models. Int. J. Plasticity (in press).

Byrne, P.M., McIntyre, J., 1994. Deformations in granular soils due to cyclic loading. In: Proceedings of Settlement 94, ASCE Geotechnical Special Publication No. 40, Texas, June, pp. 1864–1896.

Casagrande, A., 1975. Liquefaction and cyclic deformation of sands—a critical review. In: Proceedings of the 5th Pan-American Conference on Soil Mechanics and Foundation Engineering, Buenos Aires, Argentina (also published as Harvard Soil Mechanics Series No. 88, January 1976, Cambridge, MA).

Castro, G., Poulos, S.J., 1977. Factors affecting liquefaction and cyclic mobility. J. Geotechnical Engineering Division, ASCE 103 (GT6), 501–516.
Chiarelli, A.S., Shao, J.F. Modeling of elastoplastic damage behavior of a claystone. Int. J. Plasticity (in press).
Cubrinovski, M., Ishihara, K., 1998. State concept and modified elastoplasticity for sand modeling. Soils and Foundations 38 (4), 213–225.
Dafalias, Y.F., Popov, E.P., 1975. A model for nonlinearly hardening materials for complex loadings. Acta Mechanica 21, 173–192.
Dafalias, Y.F., Popov, E.P., 1977. Cyclic loading for materials with a vanishing elastic region. Nuclear Engineering and Design 41, 293–302.
Dafalias, Y.F., 1986. Bounding surface plasticity I: mathematical formulation and hypoplasticity. J. Engineering Mechanics, ASCE 112 (9), 966–987.
Dafalias, Y.F., Manzari, M.T., 1999. Modeling of fabric effect on the cyclic loading response of granular soils. In: Proceedings of ASCE 13th Engineering Mechanics Conference, 13–16 June, Baltimore, MD.
Davis, C.A., Bardet, J.P., 1996. Performance of two reservoirs during the 1994 Northridge Earthquake. J. Geotechnical Engineering, ASCE 122 (8), 613–622.
DiMaggio, F.L., Sandler, I.S., 1971. Material models for granular soils. J. Engineering Mechanics Division, ASCE 97 (EM3), 935–950.
Dobry, R., Taboada, V., Liu, L., 1995. Centrifuge modeling of liquefaction effects during earthquakes. In: Ishihara, K. (Ed.), Proceedings 1st Intl. Conf. on Earthquake Geotechnical Engineering (IS-Tokyo), Vol. 3. Balkema, Rotterdam, pp. 1291–1324.
Dobry, R., Abdoun, T., 1998. Post-triggering response of liquefied sand in the free field and near foundations. In: Dakoulas, P., Yegian, M., Holtz., R.D. (Eds.), Proceedings Geotechnical Earthquake Engineering and Soil Dynamics III, Vol. 1. Geotechnical Special Publication No. 75. ASCE, pp. 270–300.
Elgamal, A.-W., Dobry, R., Parra, E., Yang, Z., 1998. Soil dilation and shear deformations during liquefaction. In: Prakash, S. (Ed.), Proceedings 4th Intl. Conf. on Case Histories in Geotechnical Engineering, pp. 1238–1259.
Finn, W.D.L., Lee, K.W., Martin, G.R., 1977. An effective stress model for liquefaction. J. Geotechnical Engineering Division, ASCE 103, 513–533.
Hatanaka, M., Uchida, A., Ohara, J., 1997. Liquefaction characteristics of a gravelly fill liquefied during the 1995 Hyogo-Ken Nanbu earthquake. Soils and Foundations 37 (3), 107–115.
Hill, R., 1950. The Mathematical Theory of Plasticity. Oxford University Press, London, UK.
Iai, S., 1991. A Strain Space Multiple Mechanism Model for Cyclic Behavior of Sand and Its Application. Earthquake Engineering Research Note No. 43. Port and Harbor Research Institute, Ministry of Transport, Japan.
Ishihara, K., 1985. Stability of natural deposits during earthquakes. In: Proceedings, 11th International Conference on Soil Mechanics and Foundation Engineering, Vol. 2, Theme Lecture, pp. 321–376.
Iwan, W.D., 1967. On a class of models for the yielding behavior of continuous and composite systems. J. Applied Mechanics, ASME 34, 612–617.
Japanese Geotechnical Society, 1996. Special Issue on Geotechnical Aspects of the January 17 1995 Hyogoken-Nambu Earthquake. Soils and Foundations Journal.
Jeremic, B., Runesson, K., Sture, S., 1999. A model for elastic-plastic pressure sensitive materials subjected to large deformations (Invited paper). Intl. J. Solids Structures 36 (31–32), 4901–4918.
Lacy, S., 1986. Numerical Procedures for Nonlinear Transient Analysis of Two-phase Soil System. PhD Dissertation, Princeton University, NJ.
Lade, P.V., 1977. Elasto-plastic stress-strain theory for cohesionless soil with curved yield surfaces. Intl. J. Solids Structures 13, 1014–1035.
Lambe, T.W., Whitman, R.V., 1969. Soil Mechanics. John Wiley & Sons, New York.
Li, X.S., Dafalias, Y.F., 2000. Dilatancy for cohesionless soils. Geotechnique 50 (4), 449–460.
Lubliner, J., 1990. Plasticity Theory. Macmillan, New York.
Manzari, M.T., Dafalias, Y.F., 1997. A critical state two-surface plasticity model for sands. Geotechnique 49 (2), 252–272.

Mroz, Z., 1967. On the description of anisotropic work hardening. J. Mechanics and Physics of Solids 15, 163–175.

Muraleetharan, K.K., Mish, K.D., Arulanandan, K., 1994. A fully coupled nonlinear dynamic analysis procedure and its verification using centrifuge test results. Int. J. Numerical and Analytical Methods in Geomechanics 18, 305–325.

Nemat-Nasser, S., Shokooh, A., 1979. A unified approach to densification and liquefaction of cohesionless sand in cyclic shearing. Canadian Geotechnical Journal 16, 659–678.

Nemat-Nasser, S., Tobita, Y., 1982. Influence of fabric on liquefaction and densification potential of cohesionless sand. Mechanics of Materials 1, 43–62.

Nemat-Nasser, S., Zhang, J., 2002. Constitutive relations for cohesionless frictional granular materials. Int. J. Plasticity 18 (4), 531–547.

Oka, F., Yashima, A., Adachi, T., 1995. A strain localization analysis using a viscoplastic softening model for clay. Intl. J. Plasticity 11 (5), 523–545.

Oka, F., Jiang, M., Higo Y. Effects of transport of pore water and material hetrogeneity on strain localization analysis of fluid-saturated gradient dependent viscoplastic geomaterial. Int. J. Plasticity (in press).

Parra, E., 1996. Numerical Modeling of Liquefaction and Lateral Ground Deformation Including Cyclic Mobility and Dilation Response in Soil System. PhD Thesis, Dept. of Civil Engineering, Rensselaer Polytechnic Institute, Troy, NY.

Pastor, M., Zienkiewicz, O.C., 1986. A generalized plasticity hierarchical model for sand under monotonic and cyclic loading. In: Pande, G.N., Van Impe, W.F. (Eds.), Proceedings, 2nd International Conference on Numerical Models in Geomechanics. M. Jackson and Son, pp. 131–150.

Peric, D., Ayari, M.A., 2000. Influence of Lode's angle on generation of pore pressure in soils. In: Khan, A.S., Zhang, H., Yuan, Y. (Eds.), Proceedings of the Eighth International Symposium on Plasticity and its Current Applications. NEAT Press, Fulton, MD, pp. 312–314.

Peric, D., Ayari, M.A., 2002. On the analytical solutions for the three-invariant cam clay model. Int. J. Plasticity 18, 1061–1082.

Popescu, R., Prevost, J.H., 1993. Numerical class A predictions for models nos 1, 2, 3, 4a, 4b, 6, 7, 11 & 12. In: Arulanandan, K., Scott, R.F. (Eds.), Proceedings of the Intl. Conference on the Verification of Numerical Procedures for the Analysis of Soil Liquefaction Problems, Vol. 1. Balkema, Rotterdam, pp. 1105–1207.

Prevost, J.H., 1978a. Anisotropic undrained stress-strain behavior of clays. J. Geotechnical Engineering Division, ASCE 104 (GT8), 1075–1090.

Prevost, J.H., 1978b. Plasticity theory for soil stress-strain behavior. J. Engineering Mechanics Division, ASCE 104 (EM5), 1177–1194.

Prevost, J.H., 1985. A simple plasticity theory for frictional cohesionless soils. Soil Dynamics And Earthquake Engineering 4 (1), 9–17.

Prevost, J.H., 1989. DYNA1D, A Computer Program for Nonlinear Seismic Site Response Analysis: Technical Documentation. Technical Report NCEER-89–0025. National Center for Earthquake Engineering Research, State University of New York at Buffalo.

Radi, E., Bigoni, D., Loret, B., 2002. Steady crack growth in elastic-plastic fluid-saturated porous media. Intl. J. Plasticity 18 (3), 345–358.

Seed, H.B., Lee, K.L., Idriss, I.M., Makdisi, F.I., 1975. The slides on the San Fernando dams during the earthquake of February 9, 1971. J. Geotechnical Engineering Division, ASCE 101 (7), 651–688.

Seed, H.B., 1979. Soil liquefaction and cyclic mobility evaluation for level ground during earthquakes. J. Geotechnical Engineering Division, ASCE 105 (GT2), 201–255.

Seed, H.B., Seed, R.B., Harder, L.F., Jong, H.L., 1989. Reevaluation of the Slide in the Lower San Fernando Dam in the 1971 San Fernando Earthquake. Report No. UCB/EERC-88/04. University of California, Berkeley, CA.

Seed, R.B., Dickenson, S.E., Riemer, M.F., Bray, J.D., Sitar, N., Mitchell, J.K., Idriss, I.M., Kayen, R.E., Kropp, A., Hander Jr., L.F., Power, M.S., 1990. Preliminary Report on the Principal Geotechnical Aspects of the October 17, 1989, Loma Prieta Earthquake. Report No. UCB/EERC-90/05. Earthquake Engineering Research Center. University of California, Berkeley, CA.

Sitar, N. (Ed.), 1995. Geotechnical Reconnaissance of the Effects of the January 17, 1995, Hyogoken-

Nanbu Earthquake Japan. Report No. UCB/EERC-95/01. Earthquake Engineering Research Center, Berkeley, CA.

Sture, S., 1999. Constitutive issues in soil liquefaction. In: Lade, P.V., Yamamuro, J.A. (Eds.), Proceedings of the International Workshop on the Physics and Mechanics of Soil Liquefaction. Balkema, Rotterdam, pp. 133–143.

Vaid, Y.P., Thomas, J., 1995. Liquefaction and postliquefaction behavior of sand. J. Geotechnical Engineering, ASCE 121 (2), 163–173.

Vaid, Y.P., Sivathayalan, S., 1999. Fundamental factors affecting liquefaction susceptibility of sands. In: Lade, P.V., Yamamuro, J.A. (Eds.), Proceedings of the International Workshop on the Physics and Mechanics of Soil Liquefaction. Balkema, Rotterdam, pp. 105–120.

Vaunat, J., Cante, J.C., Ledesma, A., Gens, A., 2000. A stress point algorithm for an elastoplastic model in unsaturated soils. Intl. J. Plasticity 16 (2), 121–141.

Voyiadjis, G.Z., Kim, D. Finite element analysis of the piezocone test in cohesive soils using an elastoplastic-viscoplastic model and updated Lagrangian formulation. Int. J. Plasticity (in press).

Wang, Z.L., Dafalias, Y.F., Shen, C.K., 1990. Bounding surface hypoplasticity model for sand. J. Engineering Mechanics, ASCE 116, 983–1001.

Yang, Z., 2000. Numerical Modeling of Earthquake Site Response Including Dilation and Liquefaction. PhD Dissertation, Dept. of Civil Engineering and Engineering Mechanics, Columbia University, New York.

Youd, T.L., Hansen, C., Bartlett, S., 1999. Revised MLR equations for predicting lateral spread displacement. In: O'Rourke, T.D., Bardet, J.-P., Hamada, M. (Eds.), Proceedings, 7th U.S.–Japan Workshop on Earthquake Resistant Design of Lifeline Facilities and Countermeasures Against Liquefaction. Technical Report MCEER-99–0019, pp. 99–114.